Journal of the Ceramic Society of Japan 127 [4] 267-271 2019
DOI http://doi.org/10.2109/jcersj2.18202

JCS-Japan

NOTE

Reactive synthesis of porous $MgAl_2O_4$ membranes on a macroporous Al_2O_3-based ceramic tube toward cross-flow ultrafiltration

Yoko KAMATO[1] and Yoshikazu SUZUKI[1,2,†]

[1] Graduate School of Pure and Applied Sciences, University of Tsukuba, 1–1–1 Tennodai, Tsukuba, Ibaraki 305–8573, Japan
[2] Faculty of Pure and Applied Sciences, University of Tsukuba, 1–1–1 Tennodai, Tsukuba, Ibaraki 305–8573, Japan

Porous ceramic filters made of $MgAl_2O_4$ spinel are promising due to their excellent thermal and chemical stability. In this study, toward future cross-flow ultrafiltration applications, reactive synthesis of porous $MgAl_2O_4$ membranes on a macroporous Al_2O_3-based ceramic tube has been examined. Fine (0.2 μm) and coarse (0.7 μm) α-Al_2O_3 powders and two types of MgO sources, i.e., MgO (∼2.8 μm) and $MgCO_3$ (basic) [hydromagnesite $Mg_5(CO_3)_4(OH)_2{\cdot}4H_2O$] (∼5.5 μm) powders were used as starting materials for the reactive synthesis of porous $MgAl_2O_4$ membranes. For the intermediate layer, $MgCO_3$ (basic) powder was favorable as a MgO source because it can clog up the large (15 μm) pores in the Al_2O_3-based tube. Meanwhile, for the top layer, MgO powder with finer particle size was favored to obtain homogeneous layer for ultrafiltration.

Key-words : $MgAl_2O_4$ spinel, Dip-coating, Filter, Al_2O_3, Ultrafiltration

[Received November 24, 2018; Accepted February 4, 2019]

Porous ceramics filters attract increasing interest because of their excellent characteristics such as high mechanical properties, high corrosion resistance and high thermal stability. Currently, they are widely applied to drinking water purification,[1)–3)] waste liquid treatment,[4)–8)] exhaust gas filtration,[9)–12)] and so on. Thanks to their robust features, porous ceramic filters can be operated for longer time under severer conditions compared with organic membranes. Furthermore, they are reusable by the backwashing as well as by the regeneration via heat or chemical treatment.

Porous ceramics filters are generally categorized into 5 classes by their pore diameter d, i.e., (1) crude filtration ($d > \sim 10\,\mu m$), (2) microfiltration ($\sim 100\,nm < d < \sim 10\,\mu m$), (3) ultrafiltration ($\sim 10\,nm < d < \sim 100\,nm$), (4) nanofiltration ($\sim 1\,nm < d < \sim 10\,nm$) and (5) reverse osmosis ($d < 1\,nm$). A variety of porous ceramics made by partial sintering or made with pore-forming agent are widely available for the crude and microfiltrations. For the ultrafiltration, Al_2O_3, TiO_2 or ZrO_2 membranes on macroporous ceramics are commercialized (e.g., Cefilt® by NGK corporation). For the nanofiltration and the reverse osmosis, porous membranes made of zeolite or polycrystalline TiO_2 on macroporous ceramics are currently used.[13)–19)]

Recently, our group has focused on porous ceramic filters made of $MgAl_2O_4$ spinel,[20)] due to its excellent thermal and chemical stability.[21)–23)] In the previous study, porous $MgAl_2O_4$ plates (thickness of ∼ 2–3 mm and diameter of ∼30 mm) was prepared by reactive sintering of $MgCO_3$ (basic) [hydromagnesite ($Mg_5(CO_3)_4(OH)_2{\cdot}4H_2O$)] and 4-type of Al_2O_3 sources.[20)] Rod-like $MgCO_3$ (basic) micrometer-sized particles thermally decompose into MgO nanoparticles at ∼500°C, which are chemically active for the double-oxide synthesis.[24)] Even with a simple dead-end type setting, the porous $MgAl_2O_4$ filter made from a fine boehmite source exhibited good microfiltration performance to remove submicron-sized colloidal particles (i.e., simulating bacteria) from a suspension.[20)] However, the filtration efficiency was very small due to their thick and dead-end type setting. In a practical point of view, a cross-flow type filter (like a tubular commercial product) is necessary to improve the filtration efficiency.

In this study, toward future cross-flow ultrafiltration applications, reactive synthesis of porous $MgAl_2O_4$ membranes on a macroporous Al_2O_3-based ceramic tube has been examined. Coarse and fine porous $MgAl_2O_4$ membranes were prepared by repeated dip-coating method.

Table 1 summarizes the starting materials for intermediate and top $MgAl_2O_4$ layers. For the Al_2O_3 source of $MgAl_2O_4$, two types of α-Al_2O_3 powders (AKP-50 and AKP-3000, Sumitomo Chemicals Co. Ltd., Japan) were used. For the MgO source of $MgAl_2O_4$, a MgO powder (99.9% purity, Kojundo Chemical Laboratory Co. Ltd., Japan) and a $MgCO_3$ (basic) powder [$Mg_5(CO_3)_4(OH)_2{\cdot}4H_2O$, hydromagnesite, 99.9% purity, Kojundo Chemical Laboratory] were used. A commercial porous Al_2O_3-based tube (Hagi glass, A-#12, pore size: 14.7 μm) with cationic composition of Al:Si:K:Na:Fe:Ca = 62.6:31.6:3.59:1.45:0.318:0.254 (in wt% by X-ray fluorescence) was used.

† Corresponding author: Y. Suzuki; E-mail: suzuki@ims.tsukuba.ac.jp

Table 1. Starting materials (in mole fraction) for intermediate and top $MgAl_2O_4$ layers

	Sample name	MgO source	Al_2O_3 source
Intermediate layer	IL-1	MgO	α-Al_2O_3 (0.7 µm*, AKP-3000)
	IL-2	$0.5MgO + 0.1[Mg_5(CO_3)_4(OH)_2{\cdot}4H_2O]$	α-Al_2O_3 (0.7 µm*, AKP-3000)
	IL-3	$0.2[Mg_5(CO_3)_4(OH)_2{\cdot}4H_2O]$	α-Al_2O_3 (0.7 µm*, AKP-3000)
Top layer	TL-1	MgO	α-Al_2O_3 (0.2 µm*, AKP-50)
	TL-3	$0.2[Mg_5(CO_3)_4(OH)_2{\cdot}4H_2O]$	α-Al_2O_3 (0.2 µm*, AKP-50)

*Median diameter (catalog value given by the supplier).

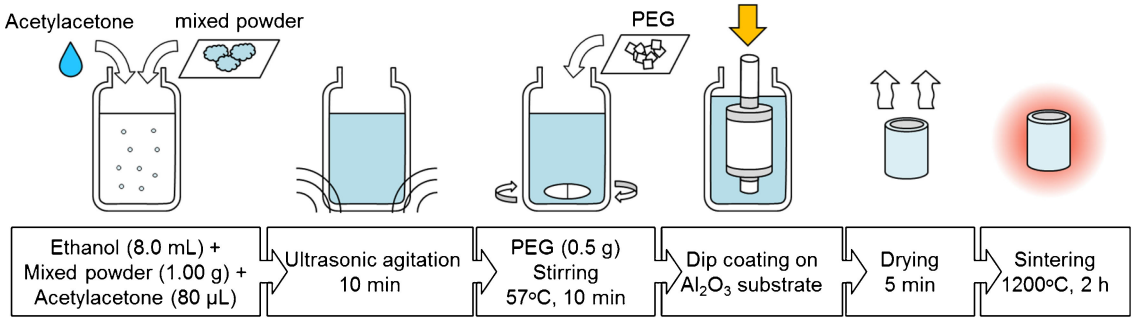

Fig. 1. Schematic illustration of sample preparation procedure.

The particle size distribution of MgO and Al_2O_3 sources was measured by dynamic light scattering (DLS, FDLS3000, Otsuka Electronics. Co.).

Figure 1 shows the sample preparation procedure. To prepare each slurry, 80 µL of acetylacetone as a dispersant was dropped into 8 mL of ethanol, and 1.00 g of raw material powder was dispersed. After putting the raw materials, ultrasonic agitation was carried out for 10 min. Thereafter, to prevent the sedimentation of the particles, and to increase the viscosity for better adhesion to the porous Al_2O_3 substrate, melted polyethylene glycol (PEG) was added and thoroughly stirred at 57°C for 10 min. Dip coating was performed on the porous Al_2O_3 substrate using the prepared slurry. When dip coating was carried out, a Teflon tape was wound around the upper and lower portions of the hollow porous tubes to prevent the slurry from entering the inside, and only the tube surface was coated. After dip coating, the samples were dried for 5 min and then sintered at 1200°C for 2 h. After the synthesis of the intermediate layer, second dip coating and sintering were carried out in the same flow to synthesize a top layer.

For the obtained samples, the constituent phases were identified by X-ray diffraction (XRD, Multiflex, Cu-Kα, 40 kV and 40 mA, Rigaku). The microstructures of the surface and cross section were observed by scanning electron microscopy (SEM, SU-70, Hitachi and JSM-5600LV, JEOL). The pore-size distribution of the whole sample (i.e., porous $MgAl_2O_4$ membranes on the macroporous Al_2O_3-based ceramic tube) was determined by mercury intrusion porosimetry (PoreMaster-60-GT, Quantachrome).

Figure 2 shows surface SEM images of the intermediate layers prepared from the three mixtures as given in Table 1. For the sample prepared with the MgO starting powder (IL-1), circular-like aggregates were observed. Such circular aggregates unevenly coated the porous Al_2O_3 substrate, and some uncovered part was also observed. With increasing the $MgCO_3$ (basic) (hydromagnesite) composition (IL-2 and 3), the surface of the intermediate layer became smoother, and the coverage of the intermediate layer became improved. The IL-3 sample was the best as an intermediate layer among the three sources.

In order to clarify the reason why the different microstructures were obtained, the particle size distributions of the MgO and Al_2O_3 sources were analyzed. **Figure 3** shows particle-size distributions of the MgO and Al_2O_3 sources measured by DLS. As can be seen in Fig. 3(a), the mode diameters of MgO and $MgCO_3$ (basic) powders were ~2.8 and ~5.5 µm, respectively. In Fig. 3(b), the finer Al_2O_3 powder (AKP-50) exhibited nearly monodispersion, and thus its mode diameter was almost the same as the median value in Table 1. Meanwhile, the coarse Al_2O_3 powder (AKP-3000) exhibited nearly bimodal dispersion in this analysis.

During the dip coating, the slurry was drawn into the porous alumina substrate (with pore size of 15 µm) by the capillary force. For IL-3, the drainage of the particles into the 15 µm pores was prevented in the vicinity of the Al_2O_3 substrate surface due to the clogging of larger $MgCO_3$ (basic) particles. Similar phenomenon should partially exist for IL-2. On the other hand, for IL-1, finer MgO particles moved more easily and they tended to form denser aggregate-like 'islands'. During the sintering, CO_2 and H_2O emissions resulted in the volume shrinkage of the intermediate layer, and then, circular aggregates formed for IL-1 (see Fig. 2).

Figure 4 shows XRD patterns on the intermediate layers on the porous Al_2O_3 tubular substrate. Peaks of $MgAl_2O_4$ as well as those of Al_2O_3 and MgO (trace) were identified. The Al_2O_3 peaks are mainly attributed to the Al_2O_3 substrate, and trace MgO peaks are attributed to unreacted MgO. For the IL-1 sample, broad peaks at ~15 and ~22° were also observed, which implies that some of

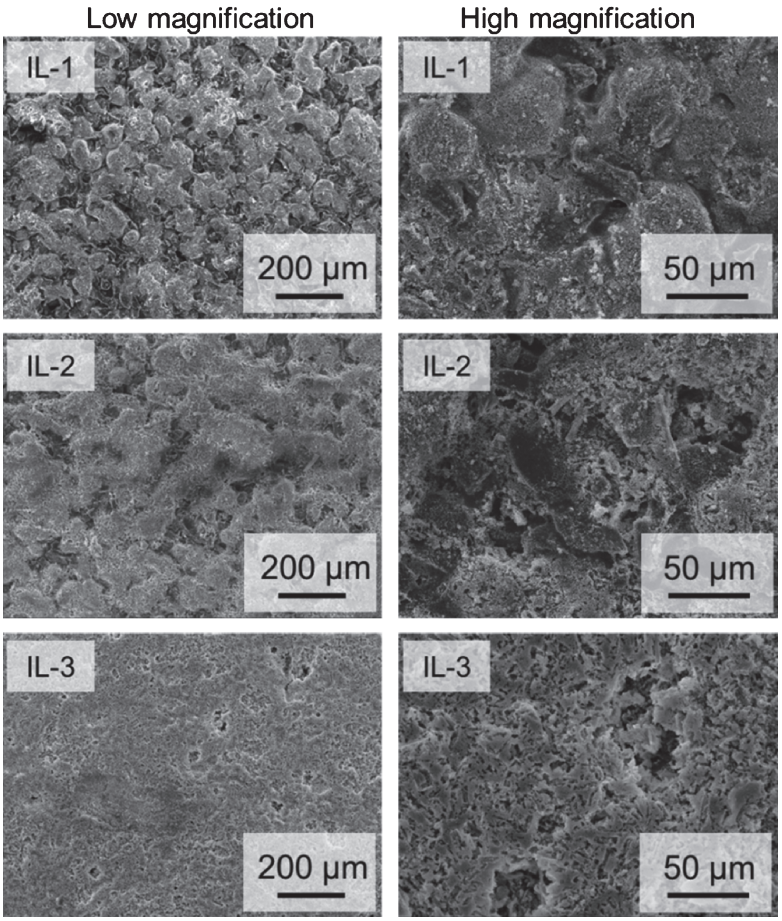

Fig. 2. SEM images of the surfaces of intermediate layers after sintering at 1200°C for 2 h.

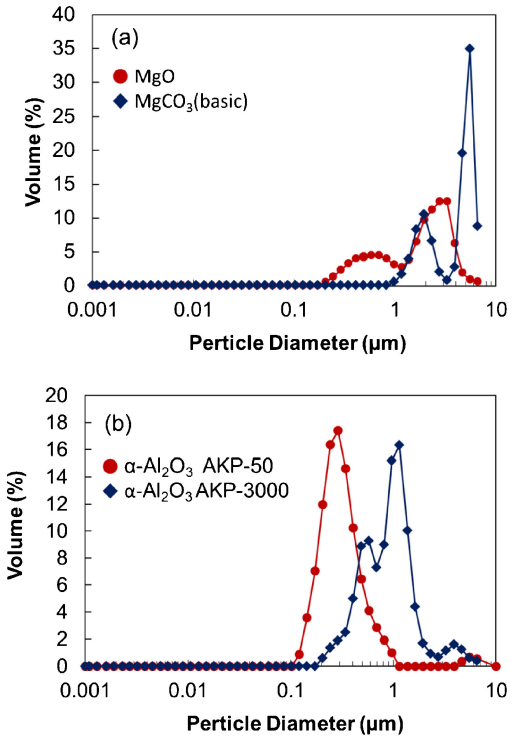

Fig. 3. Particle size distributions of (a) MgO and (b) Al_2O_3 sources measured by DLS.

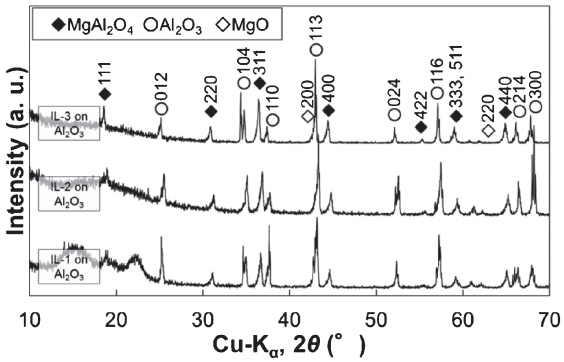

Fig. 4. XRD patterns of intermediate layers on porous (curved) Al_2O_3-based substrate. Note that due to the curvature and additives of the Al_2O_3 tubes, some peak shift may exist.

finer MgO particles were trapped in the large pores of the Al_2O_3 substrate, and they reacted with the SiO_2–K_2O–Na_2O additives in the substrate to form glassy phases.

Comparing the peak intensities of $MgAl_2O_4$, those from IL-3 [prepared from $MgCO_3$ (basic)] were the largest among three. In addition, the peak intensities of Al_2O_3, those from IL-3 were the smallest. These results well support above SEM observation (Fig. 2), i.e., the coverage of the intermediate layer IL-3 was the best in this study.

Using the IL-3 intermediate layers, two types of top layers (as filtration layer) were synthesized as shown in

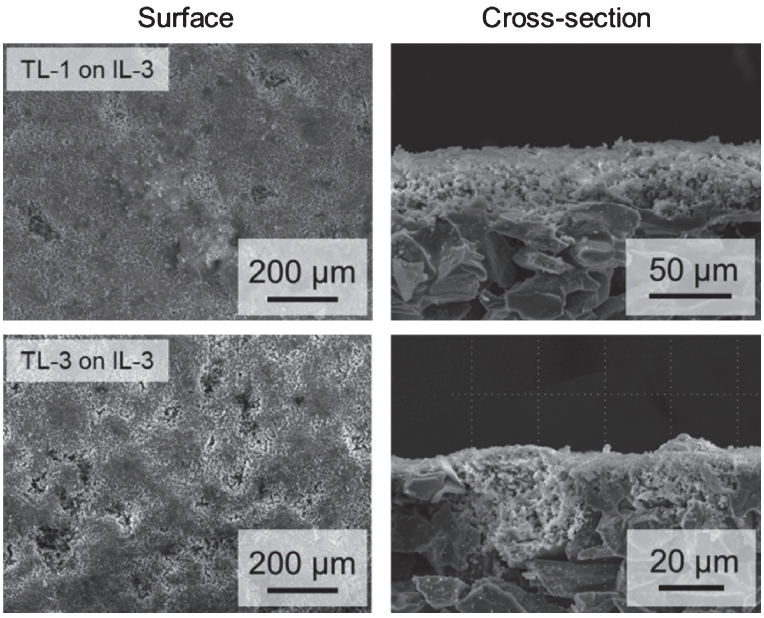

Fig. 5. SEM images of the surfaces of top layers and the cross-sections of the obtained products (i.e., porous $MgAl_2O_4$ top & intermediate membranes on the macroporous Al_2O_3-based ceramic tube).

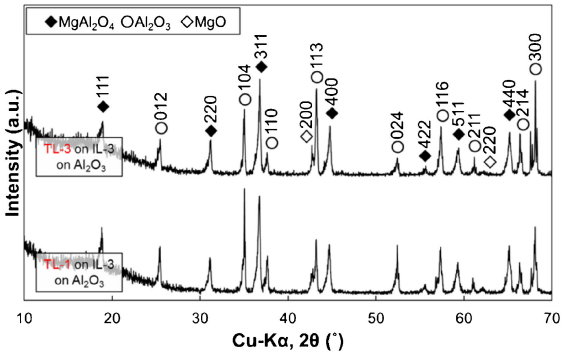

Fig. 6. XRD patterns of TL-1 and TL-3 top layers on the IL-3 intermediate layers covering porous (curved) Al_2O_3-based substrate. Note that due to the curvature and additives of the Al_2O_3 tubes, some peak shift may exist.

Fig. 5 (also see Table 1). The thickness of intermediate and top layers was ~10 and ~10 μm, respectively. By using the finer Al_2O_3 source (0.2 μm), both TL-1 (using MgO) and TL-3 [using $MgCO_3$ (basic)] were composed of fine $MgAl_2O_4$ particles. From these SEM images, the TL-1 sample apparently contained less surface defects than the TL-3 sample, probably due to the size similarity of MgO and finer Al_2O_3 sources, resulting the formation of finer and denser $MgAl_2O_4$ particles.

Figure 6 shows XRD patterns of TL-1 and TL-3 top layers on the IL-3 intermediate layers covering porous (curved) Al_2O_3-based substrate. For the TL-3 sample (using larger $MgCO_3$ (basic) as a MgO source), strong and sharp Al_2O_3 reflections were observed at higher angles (2θ~65–68°), although Al_2O_3 reflections were somewhat weaker at middle angles (2θ~33–37°). This result can probably be explained by the heterogeneous surface structure for the TL-3 on IL-3 sample (Fig. 5); X-ray can penetrate through its defect-like structure at higher angles, and XRD signals from Al_2O_3 substrate become larger. These phenomena might be related to the second shrinkage of the intermediate layer IL-3 during the sintering step for the top layer. To further elucidate the microstructure development, pore-structure analysis was conducted in a following part.

Figure 7 shows pore-size distributions determined by mercury porosimetry. As can be seen from Fig. 7(a), all three samples contained 15 μm-sized large pores, corresponding to the porous Al_2O_3 substrate. From Fig. 7(b), corresponding to the microfiltration range, pore volumes of coated samples clearly increased compared with the pristine porous Al_2O_3 tube, which is mainly attributable to the intermediate layer (see Fig. 2, IL-3). From Fig. 7(c), corresponding to the nano-and ultrafiltration range, pore volumes much increased compared with the pristine porous Al_2O_3 tube, in particular for the 10–100 nm range (right half of the figure). These results are in good agreement with the SEM observation (Fig. 5), and suggest that the porous $MgAl_2O_4$ membranes on macroporous Al_2O_3-based ceramic tubes are promising for the ultrafiltration applications.

Throughout this study, for the intermediate layer, $MgCO_3$ (basic) powder with larger particle size was favorable as a MgO source of $MgAl_2O_4$ because it can clog up the large (15 μm) Al_2O_3 pores. Meanwhile, for the top layer, MgO powder with finer particle size was somewhat favored to obtain homogeneous layer suitable for the ultrafiltration.

In this study, toward future cross-flow ultrafiltration applications, reactive synthesis of porous $MgAl_2O_4$ membranes on a macroporous Al_2O_3-based ceramic tube has been examined. Coarse and fine porous $MgAl_2O_4$ membranes were prepared by repeated dip-coating method.

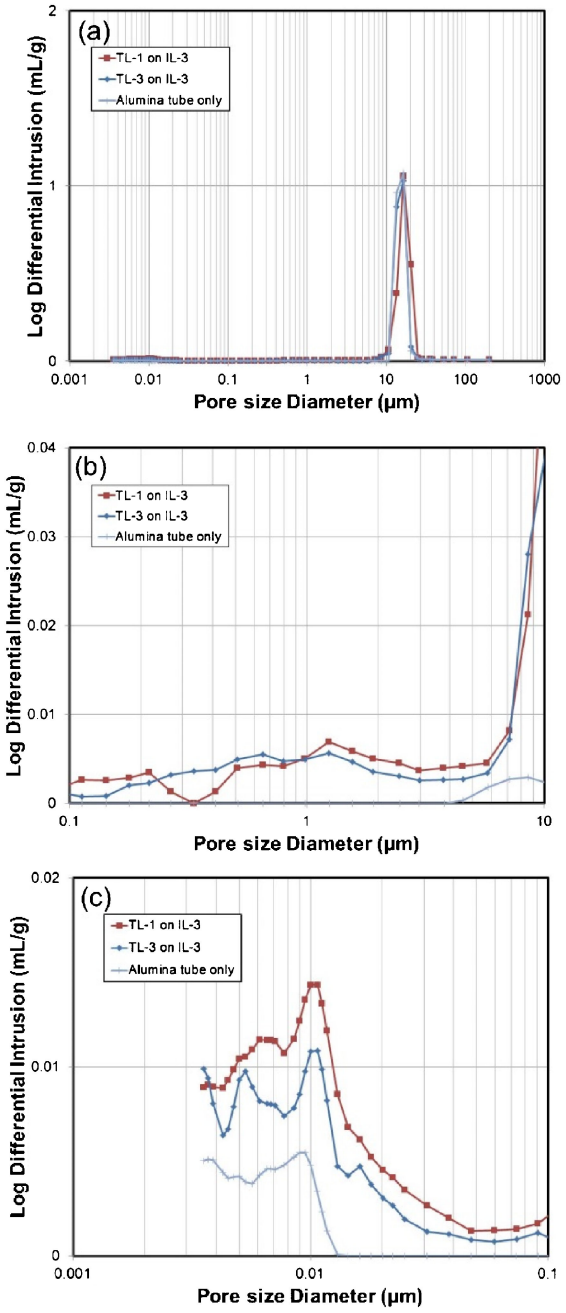

Fig. 7. Pore-size distributions determined by mercury porosimetry: (a) wide range, (b) enlargement for pore diameter d of 100 nm–10 μm (microfiltration range), and (c) enlargement for d of 1–100 nm (nano- and ultrafiltration range).

Throughout this study, for the intermediate layer, $MgCO_3$ (basic) powder with larger particle size was favorable as a MgO source of $MgAl_2O_4$ because it can clog up the large (15 μm) Al_2O_3 pores. Meanwhile, for the top layer, MgO powder with finer particle size was somewhat favored to obtain a homogeneous layer suitable for the ultrafiltration. With some optimization, the hierarchical porous structure in this study will be applicable for cross-flow ultrafiltration applications.

Acknowledgement This work was supported by JSPS KAKENHI Grant Number JP16H04212 for Basic Research: Category B, and Sumitomo Chemical Co. We thank Dr. Kosuke Uoe and his colleagues at Sumitomo Chemical Co. Ltd. for kind measurements of the mercury porosimetry. We appreciate the Open Facility Network Office, Research Facility Center for Science and Technology, University of Tsukuba, for the DLS measurement.

References

1) V. K. K. Upadhyayula, S. Deng, M. C. Mitchell and G. B. Smith, *Sci. Total Environ.*, 408, 1–13 (2009).
2) M. Sobsey, C. Stauber, L. Casanova, J. Brown and M. Elliott, *Environ. Sci. Technol.*, 42, 4261–4267 (2008).
3) A. Bottino, C. Capannell, A. Del Borghi, M. Colombino and O. Conio, *Desalination*, 141, 75–79 (2001).
4) S. M. Samaei, S. Gato-Trinidad and A. Altaee, *Sep. Purif. Technol.*, 200, 198–220 (2018).
5) F. Lin, S. Zhang, G. Ma, L. Qiu and H. Sun, *Web of Conferences ICAEER 2018*, 53, 04032 (2018).
6) L. Yu, M. Han and F. He, *Arab. J. Chem.*, 10, S1913–S1922 (2017).
7) M. T. Ravanchi, T. Kaghazchi and A. Kargari, *Desalination*, 235, 199–244 (2009).
8) S. K. Hubadillah, M. H. D. Othman, T. Matsuura, A. F. Ismail, M. A. Rahman, Z. Harun, J. Jaafar and M. Nomura, *Ceram. Int.*, 44, 4538–4560 (2018).
9) I. J. Kim, *J. Ceram. Process. Res.*, 11, 411–418 (2010).
10) Y. Suzuki and M. Morimoto, *J. Ceram. Soc. Jpn.*, 118, 819–822 (2010).
11) A. J. Pyzik and C. G. Li, *Int. J. Appl. Ceram. Tec.*, 2, 440–451 (2005).
12) A. Gómez-Martín, M. P. Orihuela, J. A. Becerra, J. Martínez-Fernández and J. Ramírez-Rico, *Mater. Design*, 107, 450–460 (2016).
13) T. Bein, *Chem. Mater.*, 8, 1636–1653 (1996).
14) A. Tavolaro and E. Drioli, *Adv. Mater.*, 11, 975–996 (1999).
15) J. Kim and B. V. Bruggen, *Environ. Pollut.*, 158, 2335–2349 (2010).
16) B. V. Bruggen, C. Vandecasteele, T. V. Gestel, W. Doyen and R. Leysen, *Environ. Prog.*, 22, 46–56 (2003).
17) S. Deville, *Adv. Eng. Mater.*, 10, 155–169 (2008).
18) A. R. Studart, U. T. Gonzenbach, E. Tervoort and L. J. Gauckler, *J. Am. Ceram. Soc.*, 89, 1771–1789 (2006).
19) E. C. Hammel, O. L.-R. Ighodaro and O. I. Okolin, *Ceram. Int.*, 40, 15351–15370 (2014).
20) Y. Kamato and Y. Suzuki, *Ceram. Int.*, 43, 14090–14095 (2017).
21) H. Mao, M. Selleby and B. Sundman, *Calphad*, 28, 307–312 (2004).
22) M. A. L. Braulio, M. Rigaud, A. Buhr, C. Parr and V. C. Pandolfelli, *Ceram. Int.*, 37, 1705–1724 (2011).
23) A. Saberi, F. Golestani-Fard, H. Sarpoolaky, M. Willert-Porada, T. Gerdes, R. Simon and C. Liebscher, *Ceram. Int.*, 35, 457–461 (2009).
24) Y. Suzuki, H. Tokoro and H. Abe, *Mater. Lett.*, 163, 43–46 (2016).